

promoting access to White Rose research papers



Universities of Leeds, Sheffield and York
<http://eprints.whiterose.ac.uk/>

This is an author produced version of a paper published in **Wear**.

White Rose Research Online URL for this paper:

<http://eprints.whiterose.ac.uk/10592>

Published paper

Gonzalez-Valadez, M., Baltazar, A., Dwyer-Joyce, R.S. (2010) *Study of interfacial stiffness ratio of a rough surface in contact using a spring model*, *Wear*, 268 (3-4), pp. 373-379

<http://dx.doi.org/10.1016/j.wear.2009.08.022>

Study of Interfacial Stiffness Ratio of a Rough Surface in Contact Using a Spring Model

M. Gonzalez-Valadez^{1,2}, R.S. Dwyer-Joyce², A. Baltazar³

¹ CIATEQ, A.C., Av. Manantiales 23-A, Parque Industrial Bernardo Quintana, Querétaro, México.
C.P. 76246.

Tel. number: +52 (442)1961500 Ext. 4225; Fax number: +52 (442) 1961500 Ext. 4231. Email address: miguel.gonzalez@ciateq.mx

² The University of Sheffield, Department of Mechanical Engineering, Mapping St., Sheffield, S1 3JD, UK.

³ CINVESTAV- Unidad Saltillo, Robotics and Advanced Manufacturing Program, Carr. Saltillo-Monterrey km 13.5, Ramos Arizpe, Coahuila, México.

Abstract

This study proposes the use of a simple spring model that relates the interfacial stiffness with the complex reflection coefficient of ultrasound in a rough contact. The spring model cannot be directly related to the real area of contact as this depends on the amount, shape and distribution of contacting asperities. However, it is clear that the model provides a non destructive tool to easily evaluate both longitudinal and shear interfacial stiffnesses and their ratio. Experimental findings indicate that the interfacial stiffness ratio K_{\parallel}/K_{σ} determined during loading/unloading cycles is sensitive to the roughness level and load hysteresis. The results deviate from the theoretical available micromechanical models, indicating that actual contacting phenomenon is more complex and other variables needed are not accounted for by the models.

Keywords: ultrasound, rough contact, interfacial stiffness

30

31 **Introduction**

32 The problem of mechanical contact of two elastic bodies has been of great interest to the
33 scientific community. This has been mainly triggered by the need to predict contact area
34 relevant in engineering to mechanical, electrical and heating conduction analysis. For two
35 nonconforming surfaces the properties of the interface depends on the random contact of the
36 surfaces. In a contact between rough surfaces only very few asperities go into contact.
37 Therefore, high local stresses take place at the individual asperity tips causing an immediate
38 plastic deformation and forming cold-welded junctions between the metal surfaces.
39 Additionally, with the application of normal loading-unloading cycles, hysteresis
40 phenomenon due to elastic and plastic deformation has been reported in the literature (i.e. [1],
41 [2], [3]).

42 The development of experimental tools to investigate rough contact has been a slow
43 ongoing process. Methods based on electrical and thermal conduction, measurement of fluid
44 flow through the contact and the neutron-graphic method are useful to calculate real contact
45 area but cannot provide an estimation of interfacial stiffness [4]. Kendall & Tabor [5] have
46 found different drawbacks with the methods based on electrical and thermal conduction as
47 well as with optical methods when used in real engineering contacts. When two nominally flat
48 specimens are pressed together by normal force, the deformation of asperities can be recorded
49 by means of an electric micrometer or by the stylus of a profilometer. However, in practical
50 applications, the results need to be refined by eliminating the effect of surface deformation in
51 the test machine. Krolkowski & Szczepek [4] indicated that using the method based on direct
52 measurements of compliance, the measurable limit of interfacial stiffness of a rough contact is
53 about $1 \text{ GPa } \mu\text{m}^{-1}$.

54 From the original independent investigations carried out by Kendall & Tabor [5] and
55 Tattersal [6], it was clear that the reflection coefficient of ultrasound can be related to the
56 interfacial stiffness of a rough contact by means of a spring model; however, it is not directly
57 related to the actual contact area as it was hypothesized in their study. Therefore, the results
58 show serious disadvantages of the method, but it can be a powerful tool when the stiffness is
59 the main parameter to assess. In fact, in this paper the ratio of tangential to normal stiffness is
60 evaluated utilizing the spring model of Kendall & Tabor [5].

61 Several theoretical approaches have been developed that can be applied to the contact
62 between two nominally flat surfaces, one smooth undeformable against a rough deformable
63 with isotropic statistical properties of roughness [7, 8, 9, 10]. Although the models work for
64 idealized shape of asperities and non-interacting assumption, an estimation of the real area of
65 contact and nominal pressure can be obtained.

66 Studies on normal stiffness have been reported more often than on shear interfacial
67 stiffness. However, the use of both normal and shear stiffness expressed as a ratio can be used
68 to determine the nature of contact [11]. The shear stiffness can be obtained from a pre-
69 stressed condition in which a normal load to the interface is followed by a small shear force.
70 This is a special case which requires only the application of a small elastic dynamic shear load
71 (pre-stressed interface). Ultrasonic shear waves applied in this way deform the interface only
72 elastically because of the small-scale loading-unloading cycle, centered on the static stress
73 [3]. Therefore, no additional plastic deformation at the asperities occurs independently of the
74 state of the deformation of asperities produced by the normal load. Berthoud and Baumberger
75 [12] reported direct measurements of shear stiffness versus displacement on a pre-stressed
76 rough interface. The experiments have provided evidence that indicates that a multi-contact
77 interface subjected to the small shear deformations has an elastic response. Ultrasonic studies
78 of shear stiffness versus load can be found in several publications [4, 13, 14, 16].

79 The ratio of interfacial stiffness ratios has been anticipated as an important parameter to
80 characterize an imperfect interface. Nagy [11] presented a comprehensive review to show
81 how this can potentially be used to distinguish perfect contact from kissing, slip, or partial
82 contact. For rough surfaces, the possibility of distinguishing welded condition has been of
83 interest. Recently, several works on the interfacial stiffness ratio from a rough interface have
84 been published [12, 15, 16] where loading and unloading cycles on the interface were applied.

85 The analysis carried out by Krolikowski & Szczepek [16] which combines the contact
86 model of Greenwood & Williamson [8] with the equation of Johnson [17] for small
87 tangential displacement, revealed that the ratio of tangential to longitudinal stiffness is solely
88 dependent on the Poisson ratio of the contacting rough surfaces. Similarly, by using the
89 equation of Hisakado & Tsukizoe [18] for small tangential displacements of contacting
90 asperities, Sherif & Kossa [15] also concluded that the ratio of stiffnesses can be calculated
91 only from the Poisson ratio of both surfaces in contact.

92 Recently, Baltazar et al. [14] described a theoretical model, similar to the previously
93 obtained by Krolikowski & Szczepek [16] and Mindlin [19], but which includes a correction
94 factor accounting for the angle of misalignment. Predictions of the model are very close to
95 those made through the Sherif & Kossa approach [15]. Additionally, a slight increase in the
96 ratio of stiffnesses observed on increasing nominal pressure was attributed to misalignment at
97 a single asperity contact. The model is again non dependent on the distribution of contact
98 asperities.

99 Yoshioka & Sholtz [20] provide a comprehensive model of elastic contact that allows for the
100 oblique contact in both the normal and shear directions. Nagy [11] worked with the original
101 approach of the model of Yoshioka & Sholtz [20] for a chi squared distribution of asperities.
102 It was found that the ratio of tangential to longitudinal stiffness is exclusively dependent on
103 the Poisson ratio of the contacting materials.

104 This work has three objectives: first, to develop a phenomenological understanding of the
 105 correlation between interfacial stiffness ultrasonically determined and the state of deformation
 106 of a rough surface; second, to determine interfacial stiffness ratio K_d/K_σ for different
 107 roughness levels; and third, to investigate the hysteretic behavior of K_d/K_σ and its relationship
 108 to the deformation of asperities at the interfaces.

109

110 **Micromechanical Description**

111 Krolikowsky and Szczepec [16] provide a mathematical formulation that incorporates the
 112 Hertz-Mindilin theory [19] and the contact model of Greenwood and Williamson [8]. The
 113 method models the complex contact between rough surfaces as a normally distributed set of
 114 elastic spheres contacting against an elastic plane of the same material loaded with a normal
 115 force f and a tangential force s [19, 21, 22]. Both mean contact pressure P , and mean
 116 tangential stress τ , are as follow

$$117 \quad P = D_s \frac{2E}{3(1-\nu^2)} R^{1/2} \sigma^{3/2} \int_t^\infty (x-t)^{3/2} \phi(x) dx, \quad (1)$$

$$118 \quad \tau = s D_s \frac{2E}{(2-\nu)(1+\nu)} R^{1/2} \sigma^{1/2} \int_t^\infty (x-t)^{1/2} \phi(x) dx, \quad (2)$$

119 where D_s is the summit density per unit area, R is the radius of curvature of the elastic sphere,
 120 E is Young's modulus, ν is the Poisson's ratio, σ is the variance of summit height distribution,
 121 x is the normalised height of summits, t is the normalised separation and $\phi(x)$ is the
 122 normalised height distribution function of the summits.

123 Thus, the normal K_σ and tangential K_τ stiffness per unit area for this model are

124
$$K_{\sigma} = -\frac{1}{\sigma} \frac{dP}{dt} = D_s \frac{E}{1-\nu^2} R^{1/2} \sigma^{1/2} \int_t^{\infty} (x-t)^{1/2} \phi(x) dx, \quad (3)$$

125
$$K_{\tau} = \frac{d\tau}{ds} = D_s \frac{2E}{(2-\nu)(1+\nu)} R^{1/2} \sigma^{1/2} \int_t^{\infty} (x-t)^{1/2} \phi(x) dx. \quad (4)$$

126 Combining Equations (3) and (4) yields the tangential to the normal contact stiffness ratio

127
$$\frac{K_{\tau}}{K_{\sigma}} = \frac{A(1-\nu)}{(2-\nu)}, \quad (5)$$

128 with $A=2$, which is also identical with that for the elementary contact previously formulated
 129 by Mindlin [19] and more recently by Johnson [7] for two spherical bodies in contact. The
 130 form of equation (5) has been corroborated in several studies which differ basically in the
 131 values of the coefficient A . For instance Sherif & Kossa [15] found a theoretical value
 132 for $A = \pi / 2$. For the model of Yoshioka & Sholtz [20], Nagy [11] obtained an approximated
 133 value for $A \approx 0.71$. In the model presented by Baltazar et al. [14], A has a changing value
 134 expressed as

135
$$A = \frac{2\xi}{\psi}, \quad (6)$$

136 where ξ and ψ are correction factors accounting for the geometrical misalignments in respect
 137 to shear and longitudinal directions, respectively [23]. The factor ψ takes values of about 1
 138 for angles below 50° assuming non-slip condition at the asperities. The factor ξ typically was
 139 found to vary between 0.6 and 0.8.

140

141 **Ultrasonic Response of a Rough Surface Contact**

142 Figure 1a schematically shows the reflection of a sound wave from a rough surface
 143 interface. At the contact region sound waves would pass through while at an air gap it would
 144 be totally reflected. The proportion of the amplitude of an incident wave that is reflected is

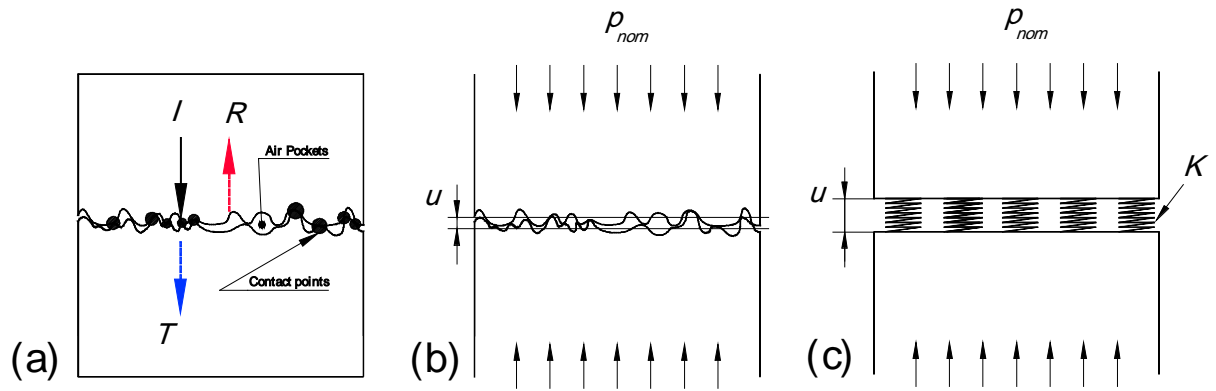
145 known as the reflection coefficient, R . Conversely, the amplitude of the incident wave
146 transmitted through the contact spots is the transmission coefficient, T (see figure 1).

147 Thus for two like materials, the reflection coefficient varies from $R=0$ for complete contact
148 to $R=1$ for no contact (i.e. a solid air interface). If the nominal pressure across the interface is
149 increased, asperity tip deformations cause both the interface to close slightly and the real area
150 of contact to increase. Kendall and Tabor [5] showed that when the wavelength of the
151 ultrasonic wave is large compared with the size of the asperity contacts, the reflection is a
152 function of the interface stiffness, K . As a consequence of the simple quasi-static spring
153 model, the reflection coefficient can be found as (shown schematically in figures 1b and 1c)

$$154 \quad R = \frac{1}{\sqrt{1 + \left(\frac{2K}{\omega z}\right)^2}}, \quad (7)$$

155 where z is the acoustic impedance of the material on either side of the interface and ω is the
156 angular frequency of the ultrasonic wave. This relationship holds for both longitudinal and
157 shear wave reflections (the longitudinal and shear wave speeds are used, respectively). A
158 similar expression exists for two dissimilar materials pressed together [24]. This model has
159 been used extensively to study the reflection and transmission of sound across incomplete
160 interfaces [2, 4, 11, 13].

161 Drinkwater et al. [25] demonstrated that the stiffness of a range of contacts of varying
162 roughness is well represented by equation (7). They studied the reflection as a function of the
163 frequency of the ultrasonic wave. The reflection coefficient was found to be dependent on
164 frequency, but the predicted stiffness was shown to be independent of frequency.



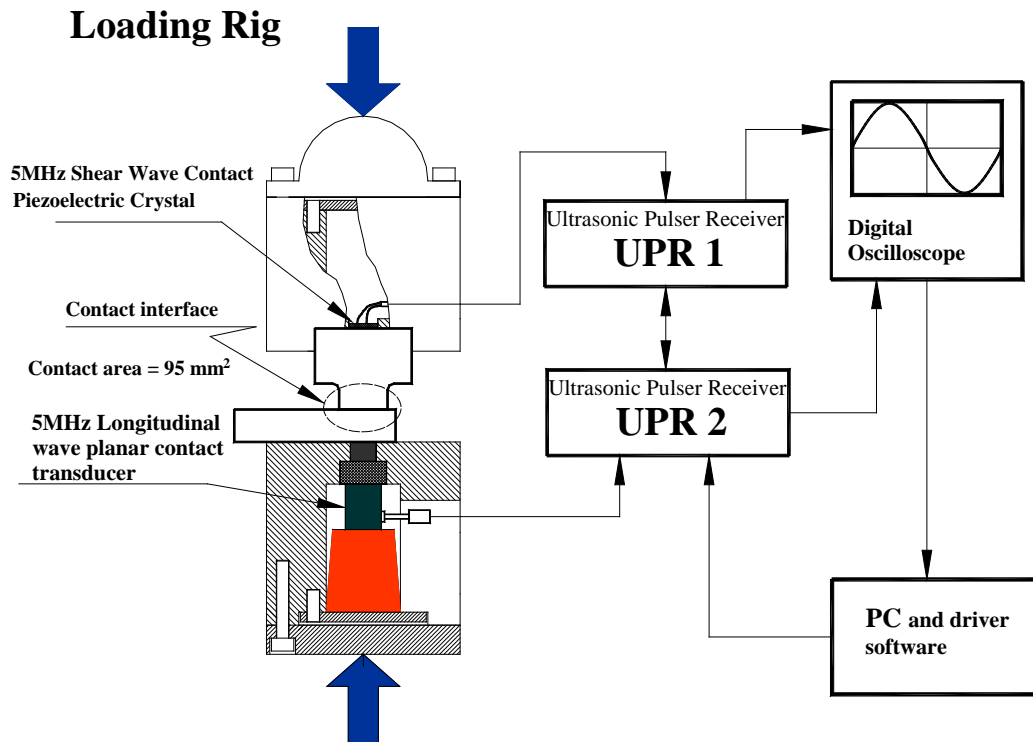
165
166
167
168

Figure 1. Scheme showing a representation of the ultrasonic response of rough surface contact, a) reflection, b) loading and deflection, and c) the spring model representation.

169 Experimental Set-up

170 Figure 2 shows the loading frame and the arrangement of the ultrasonic equipment used in
171 the tests. Two ultrasonic pulser-receivers were arranged to make it possible for the
172 longitudinal and shear signals to simultaneously be processed. The specimens were subjected
173 to loading-unloading cycles of compressive pressure in a hydraulic frame operating in load
174 control mode. The upper specimen had a disk of piezoelectric material glued to the back face
175 with a temperature stable contact adhesive. The transducer was of the wrap around electrode
176 type so both wires could be soldered directly to the top face of the $\approx 5\text{MHz}$ shear wave
177 transducer. The lower specimen was interrogated by means of a 5MHz longitudinal wave
178 planar contact transducer. The upper specimen was loaded against the lower specimen,
179 through an annulus with a hemispherical cap. The hemispherical end piece allowed the upper
180 specimen to align against the lower in order to obtain a more distributed and conformed
181 contact.

182 The contacting interfaces were made from steel specimens. The contacting face of the bottom
183 specimens were ground and polished, while those of the upper specimens were grit-blasted
184 (see Figure 3). All surfaces were measured using a surface profilometer before and after the
185 loading experiments (Table 1).



186
 187 Figure 2. Schematic diagram showing loading rig, specimens and ultrasonic measuring apparatus.
 188

189

190

191 Two ultrasonic pulser-receivers (UPR) were used to generate simultaneously voltage
 192 pulses to actuate the transducers. Both shear and longitudinal transducers had a central
 193 frequency of 5 MHz. The reflected pulses were received by the digital oscilloscope,
 194 amplified, and passed to the PC for signal processing.

195 Before both specimens are pressed together, a reference signal of ultrasound is taken. This
 196 signal is taken at the point where no contact exists. In these cases the entire incident waves,
 197 shear and longitudinal, at the interface are reflected completely (and virtually none is
 198 transmitted at the metal-air interface). The assumption that the incident wave fully reflects in
 199 an interface of solid-air, is backed by the fact that air poses very low acoustic impedance (400
 200 Ns/m^3), as opposed to steel ($47 \times 10^6 \text{Ns/m}^3$). This is the reason why air is considered a pure
 201 reflector or mirror to ultrasound. These signals are therefore equivalent to the incident signals,
 and are used as reference pulses

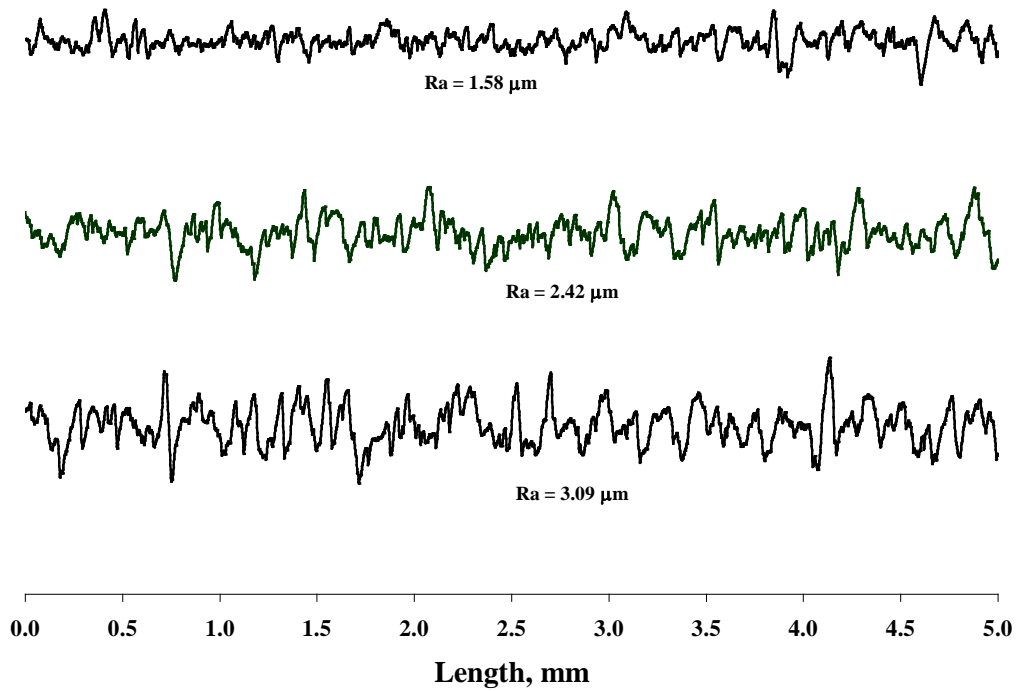


Figure 3. Different grit blasted upper specimens used in the experiment.

Material	R _a in upper specimens		R _a in bottom specimens	
	Before	After	Before	After
	Loading	Loading	Loading	Loading
Grit-blasted steel 1	1.58	1.18	0.03	0.07
Grit-blasted steel 2	2.42	1.52	0.04	0.16
Grit-blasted steel 3	3.09	1.82	0.04	0.13

Table 1. Roughness before and after test (sample length 5 mm, each result is an average of three profiles). Both specimens are made up of steel.

The test specimens are then loaded together and subsequent reflected pulses are recorded. The load is applied gradually by steps until reaching a maximum nominal pressure of 400MPa. The loading steps consist basically of applying the load from zero to the maximum with a tension-compression machine. In the same way, the unloading process is executed by decreasing the load from the maximum value to 5MPa. It should be ensured that the contact

214 interface not be downloaded completely as this would involve a different set of asperities to
215 come into contact in the next loading-unloading cycle.

216 A Fourier transform is performed on both the reflected and reference signals; dividing one
217 by the other gives the reflection coefficient spectrum. For a rough surface interface this
218 reflection coefficient depends on the frequency. Equation for the reflection coefficient
219 (Equation (7)) is then used to obtain the interfacial stiffness which should be independent of
220 frequency. In practice, there is little statistical variation due to noise in the signal, and a mean
221 stiffness is determined for all frequencies within the transducer's bandwidth. More details of
222 this method for determining interface stiffness ultrasonically can be found in Dwyer-Joyce et
223 al. [2].

224

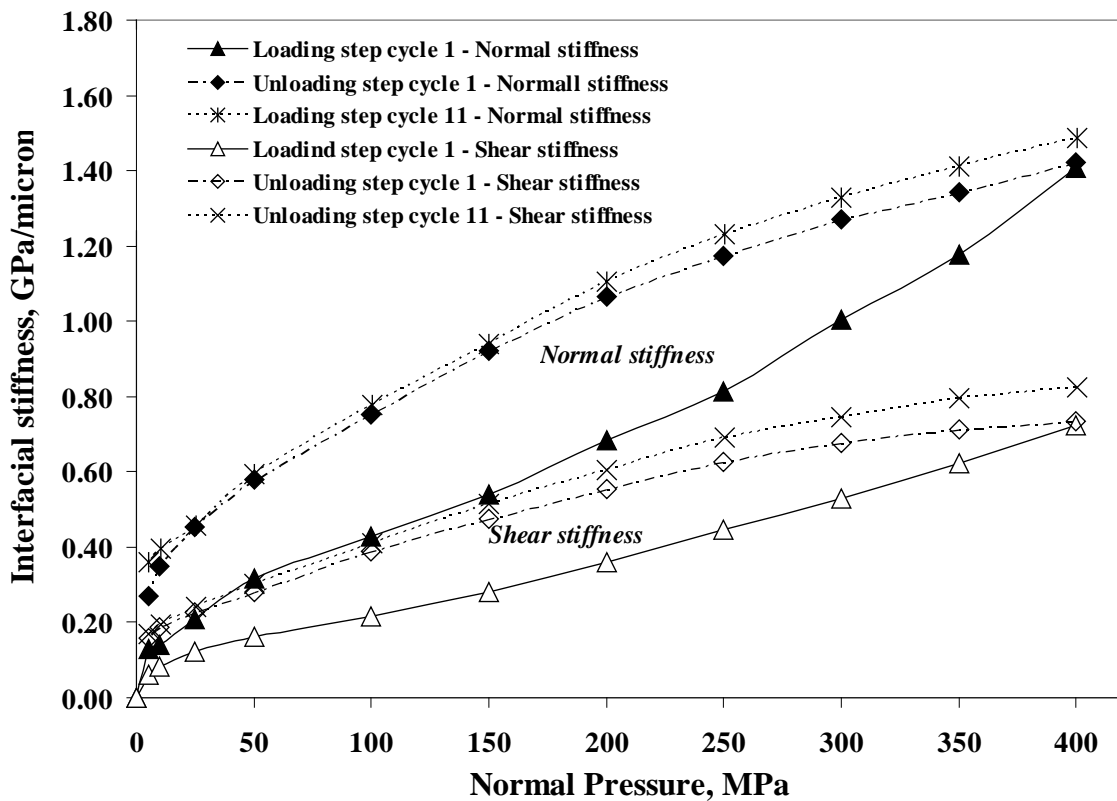
225 **Results**

226 Figures 4, 5 and 6 show the experimental results of interfacial stiffness versus normal
227 pressure. Both interfacial stiffnesses, shear and longitudinal, were calculated with equation
228 (7). Acoustical impedance z , for shear and longitudinal waves were calculated using typical
229 values of speed of sound for steel: 5900 m/s and 3100 m/s, respectively [26]. It can be
230 observed that the normal stiffness during the loading step of the first cycle in terms of normal
231 pressure follows an approximate linear relationship [27, 28]. This behaviour has previously
232 provided a simple calibration route for maps of contact stiffness and other studies [29]. It is
233 clear that to predict the normal pressure from stiffness measurement in a contacting joint, their
234 roughness has to be reproduced in laboratory specimens and the predictions would only be
235 useful for the first loading.

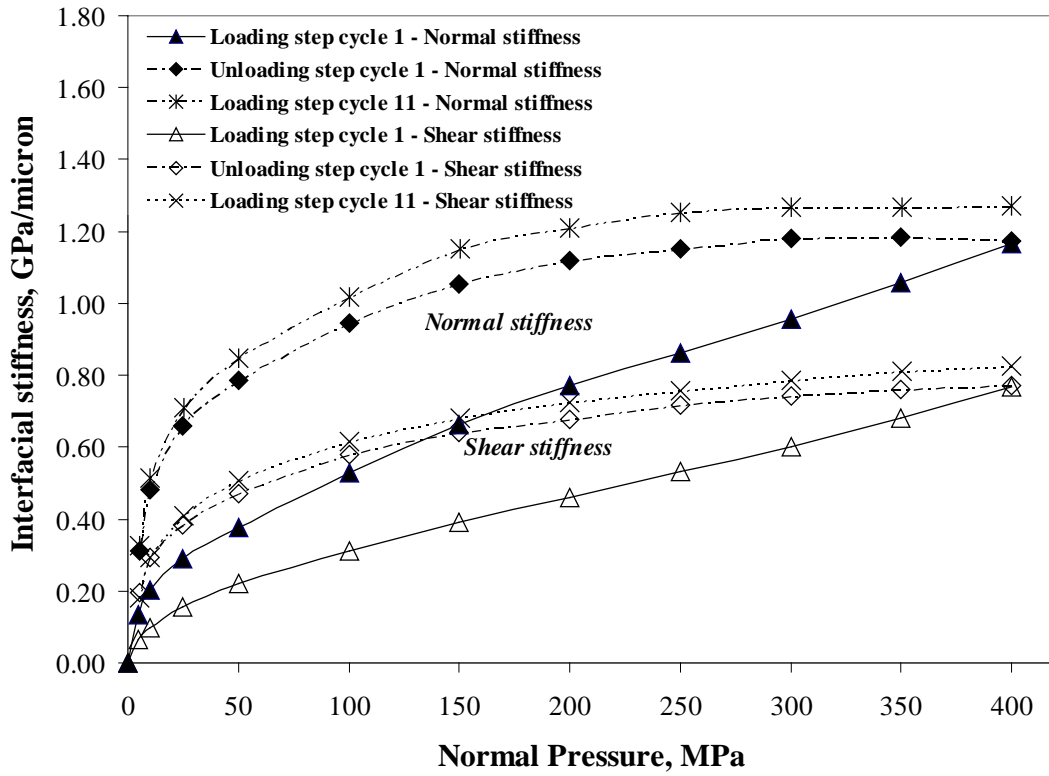
236 The curve of the unloading process in all cases follows a different path than that of the
237 loading step, showing a hysteresis phenomenon. This also indicates that most of the asperity
238 plasticity has been achieved at this stage. It has been previously recognized that the first

239 loading on the contact interface always surpasses the elasticity of asperities and therefore
 240 occurs in elasto-plastic conditions [3]. The ultrasound is not strongly affected by the plasticity
 241 of the contact, and it depends basically on the increase of contact area with load.

242 After the first loading-unloading cycle, and to ensure that remaining plasticity is fully
 243 removed and the contact is occurring in elastic conditions, 10 more complete cycles were
 244 applied. Under these conditions, the normal and shear deformations are caused by the passage
 245 of a very small displacement wave, which causes only elastic deformation. The results also
 246 show that there is a small increase in interfacial stiffness possibly due to plastic deformation
 247 being added at the end of each loading cycle. The reason for this phenomenon is not fully
 248 understood. However, in a recent study, Gonzalez & Dwyer-Joyce [30] found that two things
 249 can be producing such an effect: stress relaxation and creep which happens when a stress is
 250 sustained for a period of time.

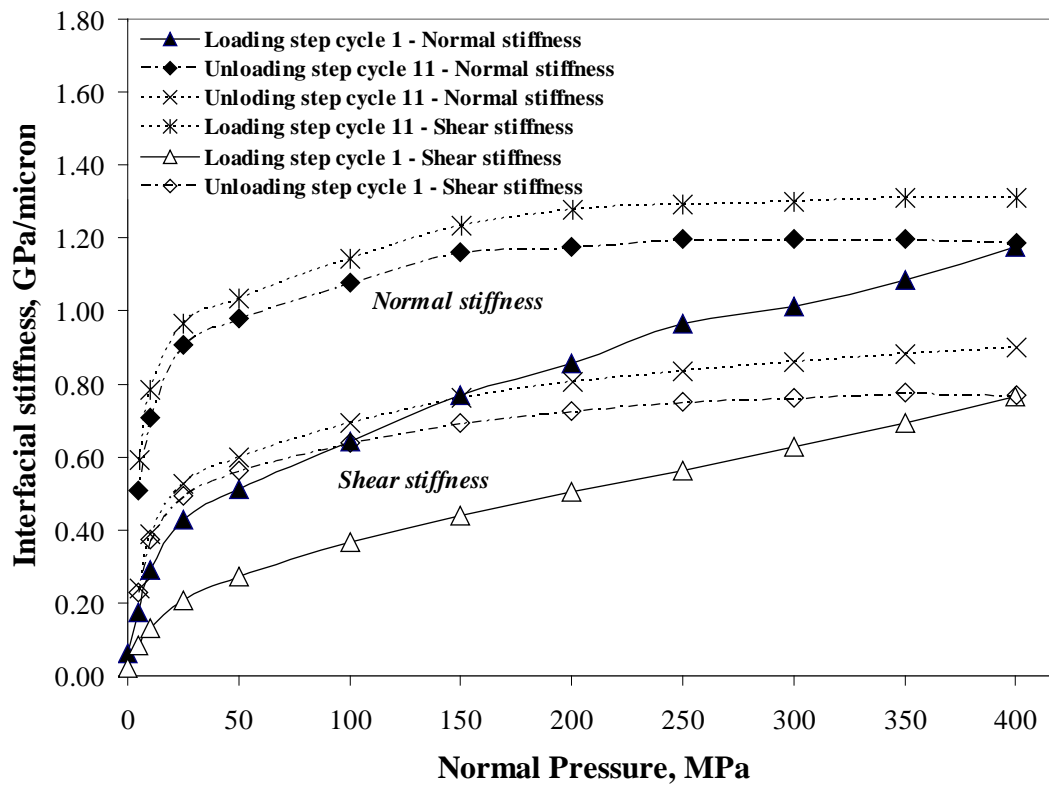


251
 252 Figure 4. Normal pressure vs. interfacial stiffness for a steel-steel interface. The upper specimen had a
 253 roughness value $R_a=1.58 \mu\text{m}$ before test.



254
255
256
257

Figure 5. Normal pressure vs. interfacial stiffness for a steel-steel interface. The upper specimen had a roughness value $R_a = 2.42 \mu\text{m}$ before test.



258
259
260

Figure 6. Normal pressure vs. interfacial stiffness for a steel-steel interface. The upper specimen had a roughness value, $R_a = 3.09 \mu\text{m}$ before test.

261 To simplify the plots, in figures 4, 5 and 6 only the curves of the loading step of cycle 11 are
262 shown. It is important to notice that one could use either the loading curve or unloading curve
263 as the values are basically the same. The values of stiffness are higher for the contact interface
264 with the least roughness. In the three different samples, the shear stiffness produces similar
265 curves to those of normal stiffness.

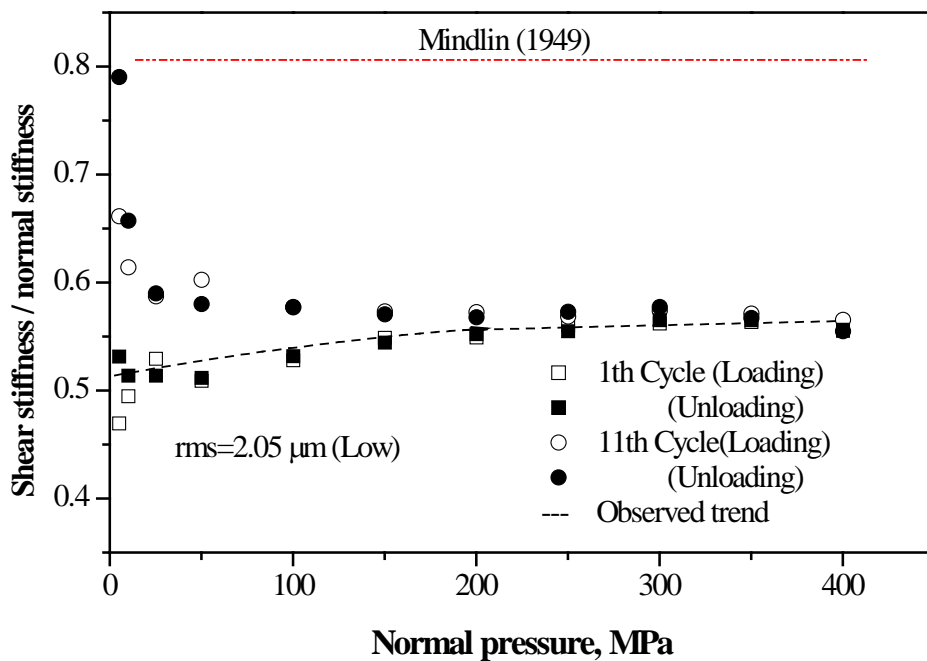
266

267 **Analysis and Discussion**

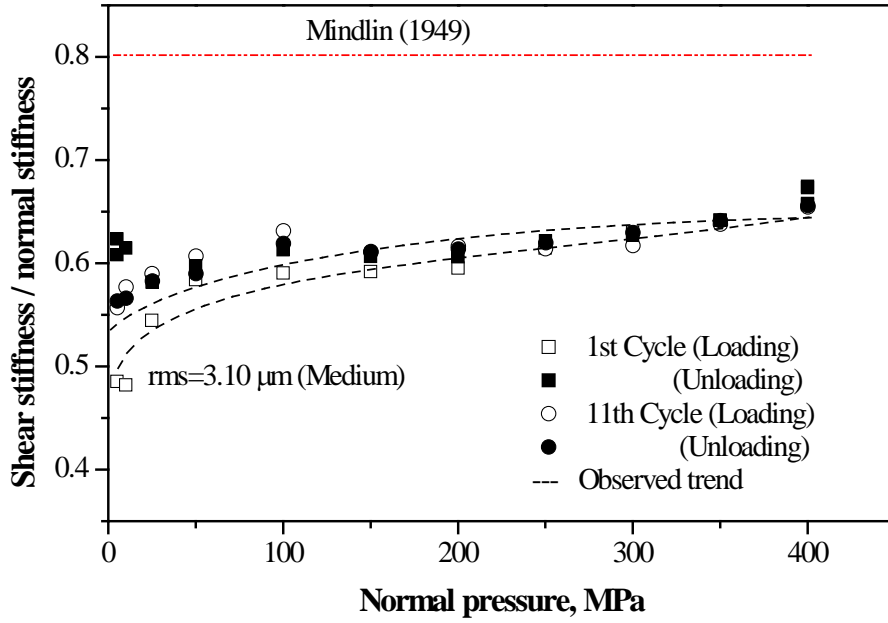
268 Figures 7- 9 show plots of longitudinal stiffness ratio as function of normal pressure. In
269 addition, the theoretical predictions found in previous literature are compared to the
270 experimental results (Figure 10). Data from the 1st and 11th loading-unloading cycles were
271 used for comparison. This makes it possible to see what happens in an elasto-plastic contact
272 (first loading-unloading cycle) and in a pure elastic contact (eleventh loading-unloading
273 cycle). Equation (5) with a Poisson ratio $\nu=0.3$ was used to estimate the theoretical
274 predictions. Our experimental results show a dependence of K_{τ}/K_{σ} ratio on load and *rms*
275 roughness. For higher values of roughness, K_{τ}/K_{σ} has a larger mean value. Also, it can be seen
276 that for high values of roughness there is an increment in the variation rate of K_{τ}/K_{σ} . Clear
277 hysteresis is observed for mild and high *rms* roughness (Figures 7 and 8), and almost none
278 detected for smooth surface. In the last case, a region of constant load independent ratio is
279 observed. The results indicate an apparent sensibility to plastic deformation during the first
280 cycles and almost none existent for additional loading cycles.

281 In the cases studied, the results deviate from the theoretical values predicted by Mindlin
282 [19]. It can be seen that only for high pressure (Figures 8 and 9) the values approach
283 theoretical ones in Eq. (5) with $A=2$. It is interesting to note that the lower ratio values are
284 always found for the first loading.

285 The results for smooth surface shows some agreement with theoretical predictions of
 286 Sherif & Kossa [15] and Baltazar et al. [14]; this last is estimated assuming an average value
 287 of the correction factor $\xi=0.7$. Only for this case, it can be suggested that the stiffness ratio is
 288 solely dependent on Poisson's ratio, and virtually constant for both elasto-plastic contact and
 289 pure elastic. The reason for the behavior which in principle could indicate a fixed relationship
 290 (i.e. load independent ratio) between normal and shear stiffness at some pressure value needs
 291 further investigation. Even though some theories agree with experimental results, it is also
 292 observed that the equation in Krolkowski & Szczeppek [16] over predicts the experimental
 293 findings of our study ($K_{\tau}/K_{\sigma}=0.82$). In contrast, the model of Yoshioka & Scholz [20]
 294 predicts values significantly lower than experimental data ($K_{\tau}/K_{\sigma}\approx 0.29$) (see Fig. 10).

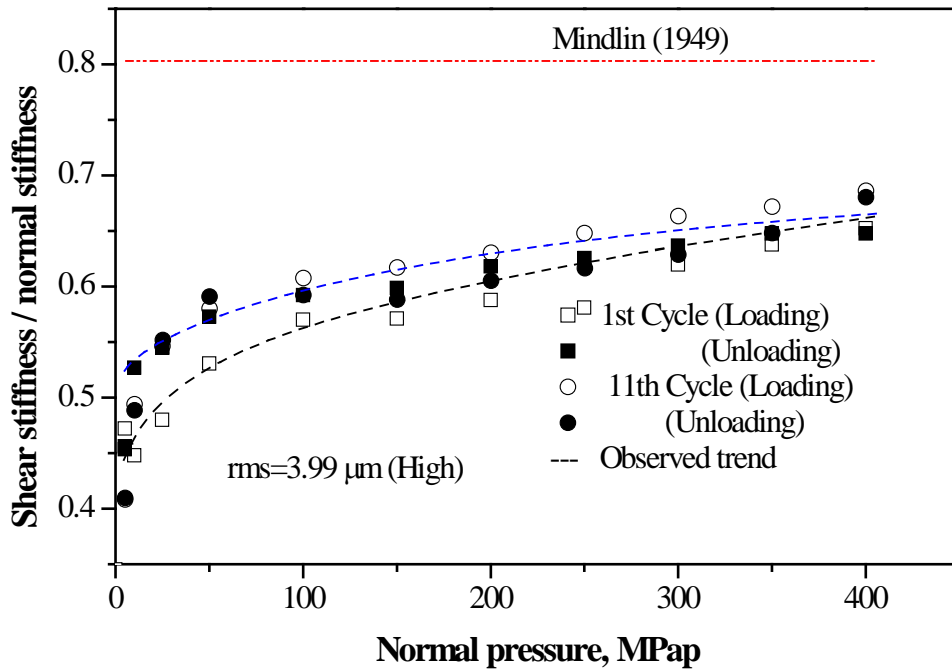


295
 296 Figure 7. Experimental results of interfacial stiffness ratio as function of loading cycles for smooth
 297 sample 1 ($R_a=1.58 \mu\text{m}$). Points indicate experimental data and the dashed line is the
 298 observed trend.
 299



300

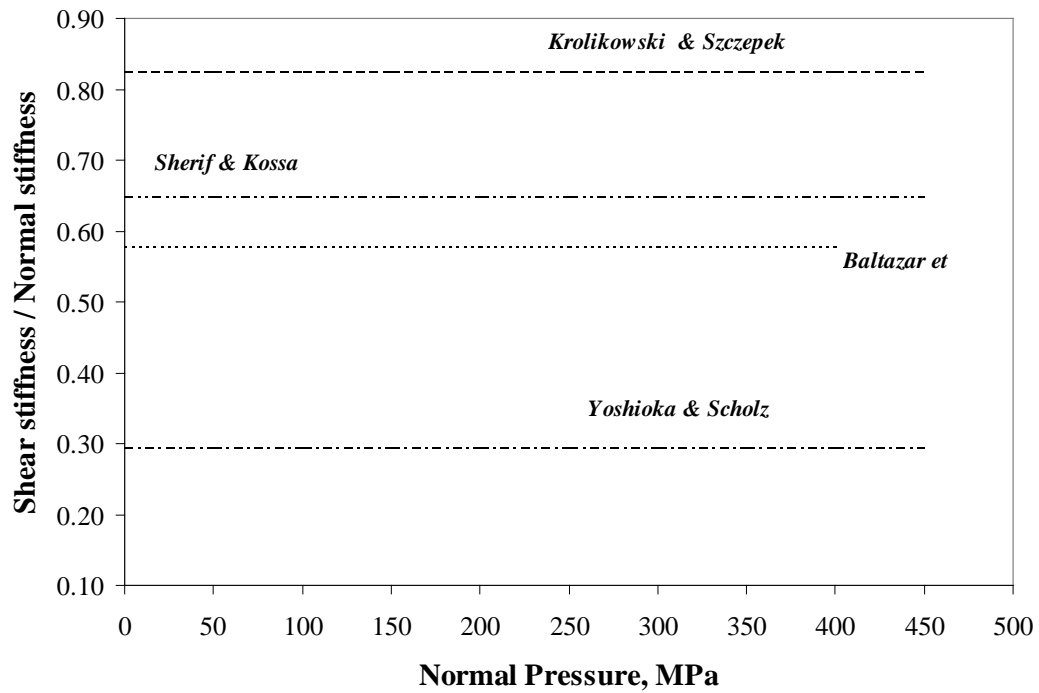
301 Figure 8. Experimental results of K_T/K_σ versus normal pressure for rough sample 2 ($Ra=2.42 \mu m$).



302

303 Figure 9. Experimental results of K_T/K_σ versus normal pressure for rough sample 3 ($Ra=3.09 \mu m$).

304



305

306 Figure 10. Theoretical predictions of shear to normal stiffness ratio.

307

308 On the other hand, ultrasonic waves are sensitive to the surface roughness but only for high
 309 frequencies when the wavelength is comparable with the height h of the interface. When this
 310 condition is not reached, QSA model can be used to describe the deformation of the interface
 311 Yalda-Mooshabad et al. [31]. In our case, the wavelength in steel for longitudinal wave and a
 312 frequency of 5MHz is about 1.18 mm. This value is much larger than the *rms* roughness of
 313 the interface.

314 From our experimental results, it is possible that an additional mechanism of wave
 315 interaction with the interface can be observed by measuring the stiffness ratio as function of
 316 pressure. In principle, two conditions could be affecting the ultrasonic reflection signature, the
 317 contact at the roughness asperities and the space (voids) left in between the asperities. It is
 318 clear that by bringing the rough surface together, the aspect ratio will change up to a point
 319 where the valleys get flatter. This condition is not accounted by the micromechanical model
 320 since it is built under the assumption of independent asperities deformation. Since the

321 observed variation of aspect ratio during loading is controlled by the contact area, it is
322 possible that the effect of voids is masked by the contact behavior and it is only unveiled
323 when the ratio $K_{\not\parallel}/K_{\sigma}$ versus pressure is estimated.

324 A review of the effect of non-interacting voids on the ultrasonic signature was given by
325 Nagy [11]. According to the study, the interfacial stiffness ratio was found to be sensitive to
326 the aspect ratio $\xi = a/b$ of spheroidal voids, where a is the out-of-plane and b the in-plane
327 dimension. It was shown that the ratio $K_{\not\parallel}/K_{\sigma}$ of two similar solids ($\nu=0.3$) in contact varies
328 monotonically from 0.45 for spherical void ($\xi \rightarrow 1$) to 0.88 for flat cracks ($\xi \rightarrow 0$).
329 Following a different approach, calculations of interfacial ratio using boundary element
330 method (BEM) and Independent Scattering Approach (ISA) were estimated by Yalda-
331 Mooshbad et al. [31]. In their calculation for an interface with a fraction area of voids of 2.5%
332 in a matrix with properties $c_l = 6.0$ Km/sec and $c_t = 3.0$ Km/sec, the ratio was found to vary
333 monotonically from 0.36 for spherical void ($\xi = 1$) to 0.76 for flat cracks ($\xi = 0.05$).

334 To estimate the mean aspect ratio in our tested surface, an approximation based on the
335 statistical parameters of the samples (Table 2) was carried out following the analysis of Nayak
336 [33]. It was found that the determined mean aspect ratio in the fresh surfaces does not change
337 considerably for samples 2 and 3, with only a decrement of about 25% for the smoothest
338 sample ($Ra=1.58\mu m$). These values of aspect ratio give a $K_{\not\parallel}/K_{\sigma}$ of about 0.78 from Nagy [11]
339 and about 0.76 from Yalda-Mooshbad et al. [31]. The values are higher than our experimental
340 findings, but it should be noted that the statistical results of samples 2 and 3 show a positive
341 correlation between experimental $K_{\not\parallel}/K_{\sigma}$ and estimated aspect ratio. However, the smooth
342 sample 1 has a lower than expected value of $K_{\not\parallel}/K_{\sigma}$ as one would predict based on its aspect
343 ratio.

344 Another relevant parameter for our study is the mean curvature which is shown
345 experimentally to vary proportional to roughness (Table 2); higher asperities are expected to

346 have larger mean curvature [32]. For fresh surfaces, the aspect ratio is a random variable,
347 which could be correlated with the distribution of asperities and curvatures [33]. If we relate
348 the values of curvature with the misalignment of contact proposed by Baltazar et al. [14], the
349 correction factor would be between 0.9-0.8 resulting in a K_r/K_σ value of about 0.65 for
350 samples 2 and 3 and a bit larger for sample 1 with a smooth surface. The result for the smooth
351 surface is in the opposite direction to the expected direction of correlation between interfacial
352 ratio and the mean curvature.
353

Sample	σ_{rms}	m_0 (μm^2)	m_2	m_4 (μm^2)	α	k_m (Degree)	d_{sum} (μm)	Aspect ratio
1	2.04	4.22	0.046	0.011	24.70	24.30	130.50	0.031
Ra=1.58 μm								
2	3.10	9.70	0.074	0.015	27.50	30.50	154.10	0.040
Ra=2.42 μm								
3	3.90	15.28	0.100	0.018	27.70	32.70	175.00	0.044
Ra=3.09 μm								

355 Table 2. Additional experimental statistical parameters for the samples studied. σ_{rms} is the
356 *rms* roughness, m_0 , m_2 , m_4 are the spectral moments of the surface, α is a parameter related
357 with the width of spectrum, k_m is the mean curvature, and d_{sum} is the mean distance between
358 summits.

359
360 From the above discussion, there is no clear evidence to indicate if any of the two proposed
361 parameters: radius of curvature or aspect ratio is solely controlling the observed stiffness ratio
362 variation during the loading cycles.

363 It is also possible that if the stiffness ratio is truly constant at the asperities contact, then
364 the ratio variations are related to change in the shape of the voids. However, the shape of the
365 voids is controlled by the contact of asperities. Therefore, any change in the contact area at
366 the asperities will control the variations of the voids. This empirical analysis could explain the
367 observed hysteresis, which is expected for large plastic deformation and correlated with the
368 larger roughness.

369 The problem is far from being resolved, and the experimental results show that the
370 micromechanics of shear contact may be more complex than expected, with that said,
371 mechanics such as slip and/or ellipsoidal contact just to mention a few, could be affecting the
372 interfacial ratio [34, 35].

373

374

375 **Conclusions**

376 An ultrasonic approach has been used to determine the normal and shear stiffness for three
377 different grit-blasted contacting surfaces. Experimental data of stiffness ratio was found to be
378 sensitive to both roughness level and plastic deformation. Degree of hysteresis for the
379 loading/unloading cycles was found to be a function of the roughness level. The assumption
380 of ultrasonic wave sensitivity to other roughness parameters such as aspect ratio of voids and
381 radius of curvature did not completely follow our experimental findings. A non-constant
382 stiffness ratio suggests that additional parameters other than those that describe the Hertzian
383 contact are being unveiled by the interfacial stiffness ratio.

384

385 **References**

- 386 1. D. Tabor, *The Hardness of Metals*, Oxford University Press, USA, 2000, p.192.
- 387 2. R.S. Dwyer-Joyce, B.W. Drinkwater, A.M. Quinn, The use of ultrasound in the investigation of
388 rough surface interfaces, *ASME Journal of Tribology* 123 (2001) 8-16.
- 389 3. J.Y. Kim, A. Baltazar, S.I. Rokhlin, Ultrasonic assessment of rough surface contact between
390 solids from elastoplastic loading-unloading hysteresis cycle, *Journal of the Mechanics and*
391 *Physics of Solids* 52 (2004) 1911-1934.
- 392 4. J. Krolikowski, J. Szczeppek, Prediction of contact parameters using ultrasonic method, *Wear*
393 148 (1991) 181-195.
- 394 5. K. Kendall, D. Tabor, An ultrasonic study of the area of contact between stationary and sliding
395 surfaces, *Proceedings of the Royal Society of London: Series A* 323 (1971) 321-340.
- 396 6. H.G. Tattersall, The ultrasonic pulse-echo technique as applied to adhesion testing, *Journal of*
397 *Applied Physics: Part D* 6 (1973) 819-832.
- 398 7. A.W. Bush, R.D. Gibson, T.R. Thomas, The elastic contact of a rough surface, *Wear* 35 (1975)
399 87-113.
- 400 8. J.A. Greenwood, J.B.P. Williamson, 1966. Contact of nominally flat surfaces, *Proceedings of*
401 *the Royal Society of London: Series A* 295 (1966) 300-319.

- 402 9. D.J. Whitehouse, J.F. Archard, The properties of random surfaces of significance in their
403 contact, *Proceedings of the Royal Society of London: Series A* 316 (1970) 97-121.
- 404 10. R.A. Onions, J.F. Archard, The contact of surfaces having a random structure, *Journal of*
405 *physics, D: Applied Physics* 6 (1973), 289-304.
- 406 11. P.B. Nagy, Ultrasonic classification of imperfect interfaces, *Journal of Nondestructive*
407 *Evaluation* 11 (1992) 127-139.
- 408 12. P. Berthoud, T. Baumberger, Shear stiffness of a solid-solid multicontact interphase, *Proceedings*
409 *of the Royal Society: Series A* 454(1998) 1615-1634.
- 410 13. R. S. Dwyer-Joyce, B. W. Drinkwater, A. M. Quinn, The Use of Ultrasound in the
411 Investigation of Rough Surface Interfaces, *Journal of Tribology*, 123 (2001) 8-17.
- 412 14. A. Baltazar, S.I. Rokhlin, C. Pecorari, On the relationship between ultrasonic and
413 micromechanical properties of contacting rough surfaces. *Journal of the Mechanics and*
414 *Physics of Solids* 50, (2002) 1397-1416.
- 415 15. H.A. Sherif, S.S. Kossa, Relationship between normal and tangential contact stiffness of
416 nominally flat surfaces, *Wear* 151 (1991) 49-62.
- 417 16. J. Krolkowski, J. Szczepek, Assessment of tangential and normal stiffness of contact between
418 rough surfaces using ultrasonic method, *Wear* 160 (1993) 253-258.
- 419 17. K.L. Johnson, *Contact Mechanics*, Cambridge University Press, New York, 1987, p.464.
- 420 18. T. Hisakado, T. Tsukizoe, Effects of distribution of surface slopes and flow pressures of
421 contact asperities on contact between solid surfaces, *Wear* 30 (1974) 213-227.
- 422 19. R.D. Mindlin, Compliance of elastic bodies in contact, *Journal of Applied Mechanics* 71
423 (1949) 259-268.
- 424 20. N. Yoshioka, C.H. Scholz, Elastic properties of contacting surfaces under normal and shear
425 loads: Part 1 – Theory, *Journal of Geophysics Research* 94 (1989) 17681-17690.
- 426 21. J.J. O'Connor, K.L. Johnson, The role of surface asperities in transmitting tangential forces
427 between metals, *Wear* 6 (1963) 118-139.
- 428 22. M. Raoof, R.E. Hobbs, Tangential compliance of rough elastic bodies in contact, *ASME*
429 *Journal of Tribology* 111 (1989) 726-729
- 430 23. K. Yamada, N. Takeda, J. Kagami, T. Naoi, Mechanisms of elastic contact and friction between
431 rough surfaces, *Wear* 48 (1978) 15-34.
- 432 24. M. Schoenberg, Elastic wave behavior across linear slip interfaces, *Journal of the Acoustical*
433 *Society of America* 68 (1980) 1516-1521.
- 434 25. B.W. Drinkwater, R.S. Dwyer-Joyce, P. Cawley, A study of the interaction between ultrasound
435 and a partially contacting solid-solid interface, *Proceedings of the Royal Society: Series A* 452

- 436 (1996) 2613-2628.
- 437 26. J. Krautkramer, H. Krautkramer, Ultrasonic Testing of Materials, Springer-Verlag, Fourth
438 Edition, 1990, p.677.
- 439 27. T. Arakawa, A study of the transmission and reflection of an ultrasonic beam at machined
440 surfaces pressed against each other, Materials Evaluation 41 (1983) 714-719.
- 441 28. K. Hodgson, The Use of Ultrasound to Investigate Engineering, Doctoral Thesis, The
442 University of Sheffield, UK, 2002.
- 443 29. M.B. Marshall, R. Lewis, B.W. Drinkwater, R.S. Dwyer-Joyce, An approach for contact stress
444 mapping in joints and concentrated contacts, Journal of Strain Analysis 39 (2004) 339-350.
- 445 30. M. Gonzalez-Valadez, R.S. Dwyer-Joyce, Asperity creep measured by the reflection of
446 ultrasound at rough surface contact, ASME Journal of Tribology 131 (2009)
447 DOI:10.1115/1.3089217.
- 448 31. I. Yalda-Mooshabad, F.J.Margetan, T.A. Gray, R.B.Thompson, Reflection of ultrasonic waves
449 from imperfect interfaces: A combined boundary element method and independent scattering
450 model approach. Journal of Nondestructive Evaluation 11(3/4) (1992) 141-149.
- 451 32. McCool, J.I. Relating profile instrument measurements to the functional performance of rough
452 surfaces, Transactions of the ASME: Journal of Tribology, 109 (1987) 264-270.
- 453 33. Nayak, P. Random process model of rough surface, Transactions of the ASME: Journal
454 of Lubrication Technology, 93 (1971) 398-407.
- 455 34. I. Sevostianov, M. Kachanov, Normal and tangential compliances of interfase of rough
456 surfaces with contacts of elliptic shape, International Journal of Solids and Structures 45 (2008)
457 2723-2736.
- 458 35. I. Sevostianov, M. Kachanov, Contact of rough surfaces: A simple model for elasticity,
459 conductivity and cross-property connections, Journal of the Mechanics and Physics of Solids
460 56 (2008) 1380-1400.